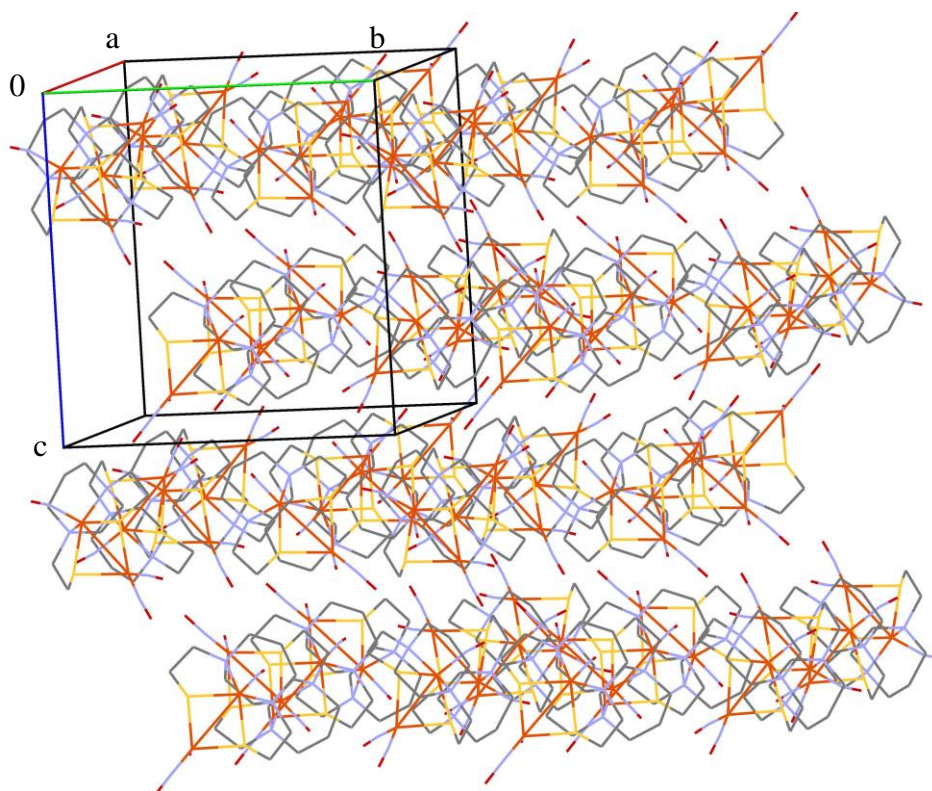
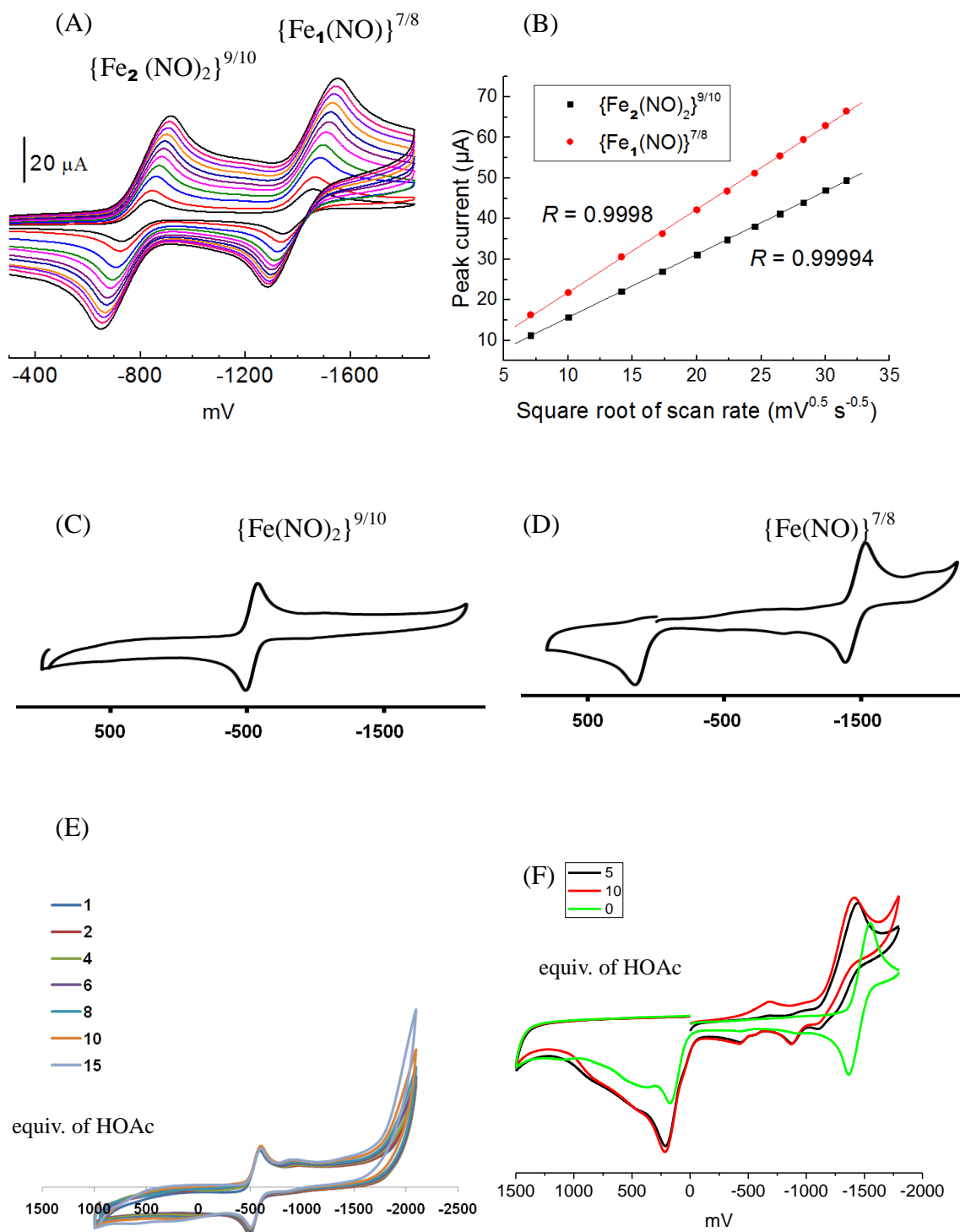


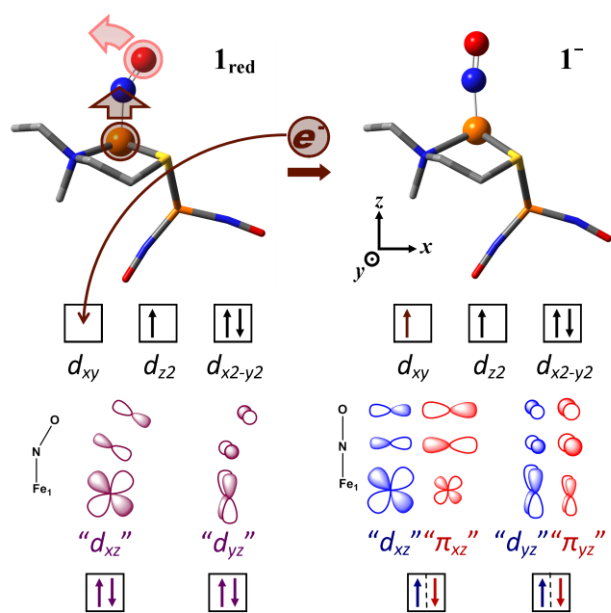
Supplementary Figure 1. Capped sticks view with atom labels and ORTEP drawing with thermal ellipsoids drawn at 50% probability of complex **1_{red}**.



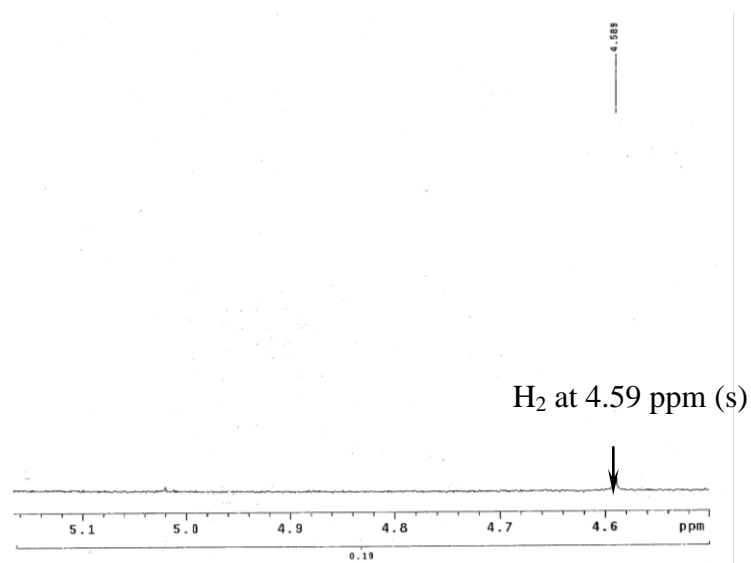
Supplementary Figure 2. The structural packing diagram of complex **1_{red}** in wireframe drawing.



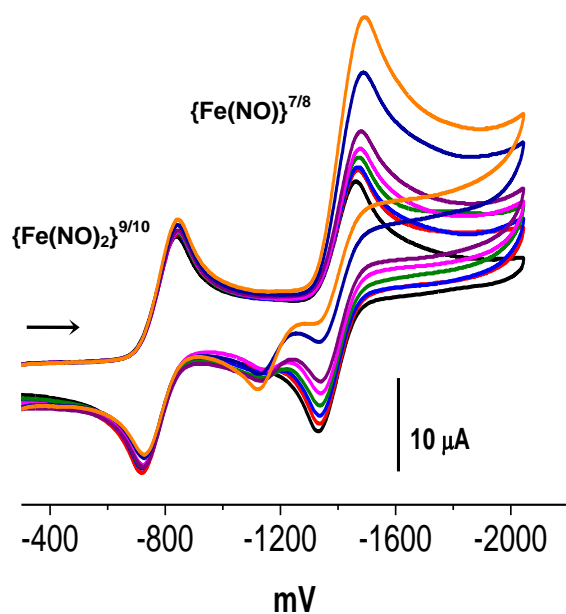
Supplementary Figure 3. (A) Cyclic voltammograms of 1^+ under different scan rates (50 - 1000 mV/s) and (B) the plot of peak currents of reduction events vs. the square roots of the scan rates. Cyclic voltammograms of (C) $(i\text{-Pr-NHC})_2Fe(NO)_2$,² (D) $(bme\text{-dach})Fe(NO)$,³ (E) addition of HOAc to $(i\text{-Pr-NHC})_2Fe(NO)_2$ and (F) addition of HOAc to $(bme\text{-dach})Fe(NO)$.



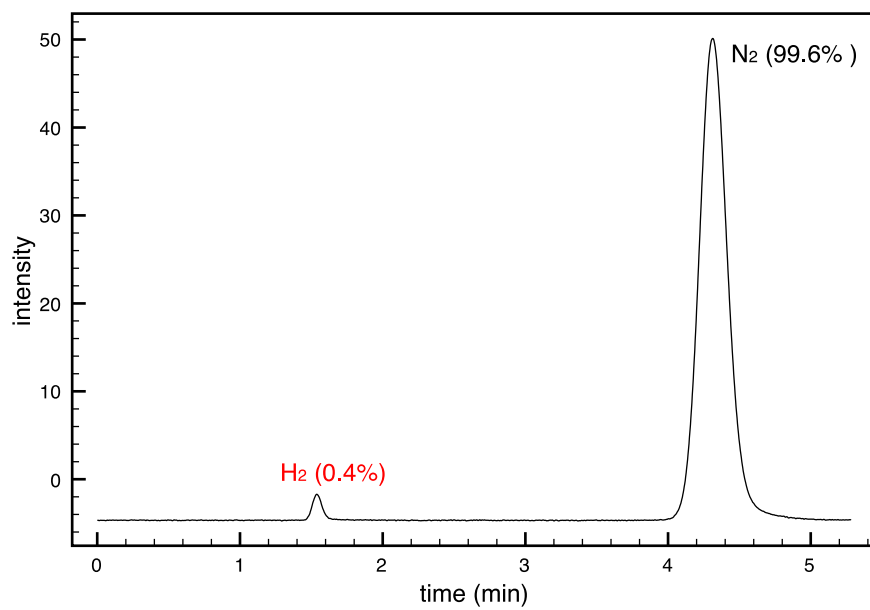
Supplementary Figure 4. Sketch of relevant geometric and electronic structure changes of the reduction of $\mathbf{1}_{\text{red}}$ to $\mathbf{1}^-$. The orbitals are represented by sketches in corresponding colors.



Supplementary Figure 5. Characterization of H₂ production from reaction of **1_{red}** and HBF₄ by ¹H NMR in CD₂Cl₂ solution.



Supplementary Figure 6. Full CV of $\mathbf{1}^+$ with increments of HOAc (0-15 equiv). Enhancement of current is observed for the $\{\text{Fe}(\text{NO})\}^{7/8}$ reduction event with the presence of weak acid, however no H_2 was detected as the product. One explanation is provided in the text. An alternative explanation is that the increased reduction current at -1.41V is likely caused by the accelerated diffusion of $\mathbf{1}^-$ from the electrode surface to bulk solution, due to the depletion of $\mathbf{1}^-$ in bulk solution by protonation, *i.e.* this is not an electrocatalytic response. Note the appearance of a new oxidative wave at -1.1V indicates growth of a new species, which is tentatively assigned as the protonated counterpart of $\mathbf{1}^-$, $\mathbf{1}\cdot\text{H}$.



Supplementary Figure 7. GC analysis of head gas after the bulk electrolysis of **1**⁺BF₄⁻ with HBF₄.

Supplementary Table 1. Crystal data for [(NO)Fe(N₂S₂)Fe(NO)₂] (**1_{red}**).

Identification code	fefe	
Empirical formula	C ₉ H ₁₈ Fe ₂ N ₅ O ₃ S ₂	
Formula weight	420.10	
Temperature	110(2) K	
Wavelength	0.71073 Å	
Crystal system	Orthorhombic	
Space group	Pbca	
Unit cell dimensions	a = 14.240(7) Å	α = 90°.
	b = 14.263(7) Å	β = 90°.
	c = 14.821(7) Å	γ = 90°.
Volume	3010.0(3) Å ³	
Z	8	
Density (calculated)	1.854 Mg/m ³	
Absorption coefficient	2.220 mm ⁻¹	
F(000)	1720	
Crystal size	0.20 x 0.20 x 0.10 mm ³	
Theta range for data collection	2.44 to 28.39°.	
Index ranges	-18<=h<=18, -18<=k<=18, -19<=l<=19	
Reflections collected	32153	
Independent reflections	3470 [R(int) = 0.0674]	
Completeness to theta = 25.00°	100.0 %	
Absorption correction	Semi-empirical from equivalents	
Max. and min. transmission	0.603 and 0.746	
Refinement method	Full-matrix least-squares on F ²	
Data / restraints / parameters	3470 / 0 / 190	
Goodness-of-fit on F ²	1.026	
Final R indices [I>2sigma(I)]	R1 = 0.0295, wR2 = 0.0671	
R indices (all data)	R1 = 0.0405, wR2 = 0.0729	
Largest diff. peak and hole	0.734 and -0.475 e.Å ⁻³	

Supplementary Table 2. Bond lengths [Å] and angles [°] for [(NO)Fe(N₂S₂)Fe(NO)₂] (**1_{red}**)

Fe1···Fe2 3.006(1) Å	C6-H6A 0.9900 Å
Fe1-N5 1.692(2) Å	C6-H6B 0.9900 Å
Fe1-N2 2.034(2) Å	C7-H7A 0.9900 Å
Fe1-N1 2.038(2) Å	C7-H7B 0.9900 Å
Fe1-S1 2.2416(11) Å	C8-C9 1.507(4) Å
Fe1-S2 2.2495(11) Å	C8-H8A 0.9900 Å
Fe2-N3 1.654(2) Å	C8-H8B 0.9900 Å
Fe2-N4 1.663(2) Å	C9-H9A 0.9900 Å
Fe2-S1 2.3238(13) Å	C9-H9B 0.9900 Å
Fe2-S2 2.3377(12) Å	N5-Fe1-N2 108.00(10) ^o
S1-C1 1.840(3) Å	N5-Fe1-N1 107.33(10) ^o
S2-C9 1.843(3) Å	N2-Fe1-N1 79.18(8) ^o
O1-N3 1.198(3) Å	N5-Fe1-S1 101.47(8) ^o
O2-N4 1.198(3) Å	N2-Fe1-S1 150.28(6) ^o
O3-N5 1.171(3) Å	N1-Fe1-S1 88.59(6) ^o
N1-C6 1.498(3) Å	N5-Fe1-S2 103.17(8) ^o
N1-C2 1.497(3) Å	N2-Fe1-S2 88.59(7) ^o
N1-C3 1.498(3) Å	N1-Fe1-S2 149.33(6) ^o
N2-C8 1.496(3) Å	S1-Fe1-S2 88.43(3) ^o
N2-C7 1.495(3) Å	N3-Fe2-N4 118.37(11) ^o
N2-C5 1.500(3) Å	N3-Fe2-S1 110.63(8) ^o
C1-C2 1.506(3) Å	N4-Fe2-S1 112.20(8) ^o
C1-H1A 0.9900 Å	N3-Fe2-S2 113.52(7) ^o
C1-H1B 0.9900 Å	N4-Fe2-S2 112.78(8) ^o
C2-H2A 0.9900 Å	S1-Fe2-S2 84.43(2) ^o
C2-H2B 0.9900 Å	C1-S1-Fe1 98.33(8) ^o
C3-C4 1.521(4) Å	C1-S1-Fe2 105.85(9) ^o
C3-H3A 0.9900 Å	Fe1-S1-Fe2 82.35(2) ^o
C3-H3B 0.9900 Å	C9-S2-Fe1 98.43(9) ^o
C4-C5 1.517(4) Å	C9-S2-Fe2 107.52(10) ^o
C4-H4A 0.9900 Å	Fe1-S2-Fe2 81.87(2) ^o
C4-H4B 0.9900 Å	C6-N1-C2 111.84(18) ^o
C5-H5A 0.9900 Å	C6-N1-C3 109.69(18) ^o
C5-H5B 0.9900 Å	C2-N1-C3 107.48(19) ^o
C6-C7 1.543(3) Å	C6-N1-Fe1 104.18(14) ^o

C2-N1-Fe1 112.47(14)^o
C3-N1-Fe1 111.21(14)^o
C8-N2-C7 111.1(2)^o
C8-N2-C5 108.19(19)^o
C7-N2-C5 110.57(19)^o
C8-N2-Fe1 112.45(15)^o
C7-N2-Fe1 103.72(14)^o
C5-N2-Fe1 110.82(15)^o
O1-N3-Fe2 174.8(2)^o
O2-N4-Fe2 167.5(2)^o
O3-N5-Fe1 154.74(19)^o
C2-C1-S1 109.46(17)^o
C2-C1-H1A 109.8^o
S1-C1-H1A 109.8^o
C2-C1-H1B 109.8^o
S1-C1-H1B 109.8^o
H1A-C1-H1B 108.2^o
N1-C2 C1-111.67(19)^o
N1-C2-H2A 109.3^o
C1-C2-H2A 109.3^o
N1-C2-H2B 109.3^o
C1-C2-H2B 109.3^o
H2A-C2-H2B 107.9^o
N1-C3-C4 113.2(2)^o
N1-C3-H3A 108.9^o
C4 C3 H3A 108.9^o
N1-C3-H3B 108.9^o
C4-C3-H3B 108.9^o
H3A-C3-H3B 107.8^o
C5-C4-C3 115.8(2)^o
C5-C4-H4A 108.3^o
C3-C4-H4A 108.3^o
C5-C4-H4B 108.3^o
C3-C4-H4B 108.3^o
H4A C4 H4B 107.4^o
N2-C5-C4 113.2(2)^o
N2-C5-H5A 108.9^o
C4-C5-H5A 108.9^o
N2 C5 H5B 108.9^o
C4-C5-H5B 108.9^o
H5A-C5-H5B 107.8^o
N1-C6-C7 110.29(19)^o
N1-C6-H6A 109.6^o
C7-C6-H6A 109.6^o
N1-C6-H6B 109.6^o
C7-C6-H6B 109.6^o
H6A-C6-H6B 108.1^o
N2-C7-C6 110.88(19)^o
N2-C7-H7A 109.5^o
C6-C7-H7A 109.5^o
N2-C7-H7B 109.5^o
C6-C7-H7B 109.5^o
H7A-C7-H7B 108.1^o
N2-C8-C9 112.3(2)^o
N2-C8-H8A 109.2^o
C9-C8-H8A 109.2^o
N2-C8-H8B 109.1^o
C9-C8-H8B 109.2^o
H8A-C8-H8B 107.9^o
C8-C9-S2 109.24(19)^o
C8-C9-H9A 109.8^o
S2-C9-H9A 109.8^o
C8-C9-H9B 109.8^o
S2-C9-H9B 109.8^o
H9A-C9-H9B 108.3^o

Supplementary Table 3. Calculated $\nu(\text{NO})$ IR frequencies and geometric parameters compared with experimental values (italics).

	Energy / Kcal·mol ⁻¹	$\nu(\text{NO})$ / cm ⁻¹	$A(\text{Fe-N-O})^c$ / °	$R(\text{N-O})^c$ / Å	$R(\text{Fe}_1\text{-Fe}_2)$ / Å	$R(\text{Fe}_1\text{-N})$ / Å	$R(\text{Fe}_1\text{-(}\mu\text{-S)})$ / Å	$R(\text{Fe}_2\text{-(}\mu\text{-S)})$ / Å
[(NO)Fe(N₂S₂)Fe(NO)₂]⁺ (1⁺)								
<i>Experimental Values</i> ^a	-	<i>1806, 1770, 1746</i>	<i>165.8, 174.4, 166.6</i>	<i>1.147, 1.174, 1.169</i>	<i>2.788</i>	<i>2.026, 2.037</i>	<i>2.259, 2.244</i>	<i>2.247, 2.252</i>
Broken-symmetry Singlet	Ground	1858, 1816, 1771	164.0, 178.0, 164.2	1.168, 1.163, 1.178	2.710	2.066, 2.066	2.259, 2.259	2.242, 2.242
Closed-shell Singlet	+ 0.26	1863, 1820, 1768	164.5, 179.5, 163.4	1.168, 1.163, 1.178	2.659	2.067, 2.067	2.247, 2.247	2.229, 2.229
Triplet	+ 7.53	1850, 1789, 1781	155.8, 169.2, 172.1	1.169, 1.164, 1.176	2.925	2.056, 2.056	2.290, 2.290	2.307, 2.307
[(NO)Fe(N₂S₂)Fe(NO)₂] (1_{red})								
<i>Experimental Values</i> ^b	-	<i>1690, 1662, 1640</i>	<i>154.7, 167.5, 174.8</i>	<i>1.171, 1.198, 1.198</i>	<i>3.006</i>	<i>2.034, 2.038</i>	<i>2.250, 2.242</i>	<i>2.338, 2.324</i>
Doublet	Ground	1766, 1677, 1662	148.8, 171.6, 172.1	1.191, 1.183, 1.203	2.862	2.061, 2.061	2.250, 2.250	2.302, 2.302
Quartet	+ 4.52	1779, 1723, 1699	162.3, 167.6, 178.4	1.186, 1.179, 1.194	2.790	2.288, 2.288	2.355, 2.356	2.306, 2.307
[(NO)Fe(N₂S₂)Fe(NO)₂]⁻ (1⁻)								
Singlet	+ 9.18	1681, 1595, 1442	124.8, 165.5, 175.6	1.231, 1.202, 1.220	2.965	2.056, 2.056	2.256, 2.256	2.355, 2.355
Triplet	Ground	1693, 1625, 1611	172.3, 166.8, 173.1	1.211, 1.200, 1.216	3.075	2.327, 2.327	2.338, 2.338	2.351, 2.351

a. See reference 1 in SI.

b. This work.

c. The three parameters of three NO are listed in order: the first value is for NO from Fe₁(NO), the second and third values are NO from Fe₂(NO)₂, where the last value is for that NO which is underneath the N₂S₂ plane.

Supplementary Table 4. Experimental g -values and HFC (hyperfine coupling) parameters for [(bme-dach)Fe(NO)] and $\mathbf{1}_{\text{red}}$. Best fits were obtained on assuming two contributing species.

	$g(x, y, z)^a$ $g\text{-strain}(x, y, z)$	HFC ^a (Fe ₁ -NO)(x, y, z), MHz	
		Species I (90%)	Species II (10%) ^b
[(bme-dach)Fe(NO)]	(2.00387, 2.04187, 2.07425) (0.004, 0.002, 0.004)	(71, 27, 61)	(129, 47, 120)
$\mathbf{1}_{\text{red}}$	(1.99887, 2.03387, 2.06525) (0.000, 0.002, 0.008)	(71, 27, 61)	(129, 59, 130)

- a. The g - and hyperfine tensors are assumed to be aligned.
b. The same g -tensor is used as for the corresponding main species.

Supplementary Table 5. Predicted energies for three complexes $\mathbf{1}^+$, $\mathbf{1}_{\text{red}}$, $\mathbf{1}^-$ by two basis sets.

Basis Set	Relative Energy / (Kcal·mol ⁻¹) ^a						
	$\mathbf{1}^+$			$\mathbf{1}_{\text{red}}$		$\mathbf{1}^-$	
	BS singlet	CS singlet	triplet	Doublet	Quartet	Singlet	Triplet
All-e	0	+0.26	+7.53	0	+4.52	+9.18	0
ECP	0	+3.15	+4.69	+2.83	0	+15.87	0

a. The energy is scaled with respect to the lowest state of every complex.

Supplementary Table 6. ECP calculated $\nu(\text{NO})$ IR frequencies and geometric parameters compared with experimental values (italics).

	Energy	$\nu(\text{NO})$	$A(\text{Fe-N-O})^c$	$R(\text{N-O})^c$	$R(\text{Fe}_1\text{-Fe}_2)$	$R(\text{Fe}_1\text{-N})$	$R(\text{Fe}_1\text{-(}\mu\text{-S)})$	$R(\text{Fe}_2\text{-(}\mu\text{-S)})$
	/ Kcal·mol ⁻¹	/ cm ⁻¹	/ °	/ Å	/ Å	/ Å	/ Å	/ Å
[(NO)Fe(N ₂ S ₂)Fe(NO) ₂] ⁺ (1 ⁺)								
<i>Experimental Values</i> ^a	-	<i>1806, 1770, 1746</i>	<i>165.8, 174.4, 166.6</i>	<i>1.147, 1.174, 1.169</i>	<i>2.788</i>	<i>2.026, 2.037</i>	<i>2.259, 2.244</i>	<i>2.247, 2.252</i>
Broken-symmetry	Ground	1855, 1809, 1776	161.9, 175.8, 165.5	1.168, 1.162, 1.176	2.819	2.067, 2.067	2.288, 2.288	2.283, 2.283
Singlet								
Closed-shell	+ 3.15	1862, 1818, 1766	164.3, 179.4, 163.5	1.168, 1.163, 1.178	2.658	2.071, 2.071	2.255, 2.254	2.235, 2.235
Singlet								
Triplet	+ 4.69	1852, 1789, 1782	155.8, 171.1, 170.8	1.169, 1.163, 1.175	2.983	2.060, 2.060	2.301, 2.301	2.334, 2.334
[(NO)Fe(N ₂ S ₂)Fe(NO) ₂] (1 _{red})								
<i>Experimental Values</i> ^b	-	<i>1690, 1662, 1640</i>	<i>154.7, 167.5, 174.8</i>	<i>1.171, 1.198, 1.198</i>	<i>3.006</i>	<i>2.034, 2.038</i>	<i>2.250, 2.242</i>	<i>2.338, 2.324</i>
Doublet	Ground ^d	1763, 1678, 1659	149.3, 171.3, 172.3	1.190, 1.183, 1.203	2.889	2.067, 2.067	2.258, 2.258	2.316, 2.316
Quartet	-2.83 ^d	1778, 1723, 1696	163.7, 169.2, 176.9	1.187, 1.178, 1.192	2.803	2.291, 2.291	2.390, 2.391	2.324, 2.325
[(NO)Fe(N ₂ S ₂)Fe(NO) ₂] ⁻ (1 ⁻)								
Singlet	+15.87	1684, 1596, 1441	124.8, 165.8, 174.9	1.231, 1.201, 1.220	2.972	2.062, 2.062	2.265, 2.265	2.370, 2.370
Triplet	Ground	1693, 1620, 1608	168.1, 167.0, 172.7	1.211, 1.200, 1.216	3.105	2.330, 2.330	2.365, 2.365	2.373, 2.373

a. See reference 1 in SI.

b. This work.

c. The three parameters of three NO are listed in order: the first value is for NO from Fe₁(NO), the second and third values are NO from Fe₂(NO)₂, where the last value is for that NO which is underneath the N₂S₂ plane.

d. Though the energy is lower, its over-compact geometry is deviated from the crystal and no other evidence is available to support it as the ground state.

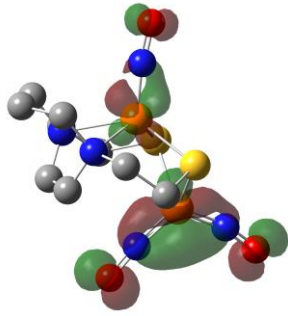
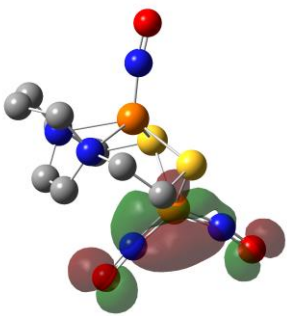
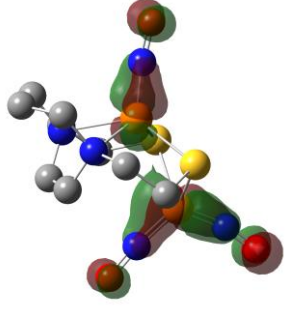
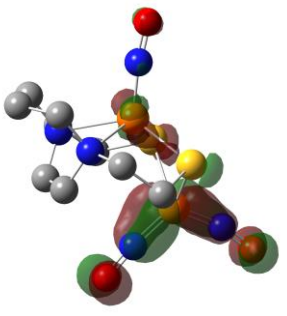
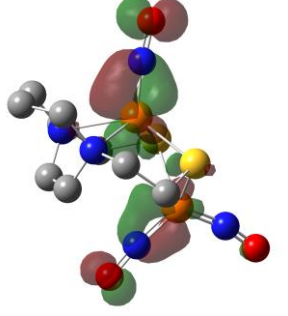
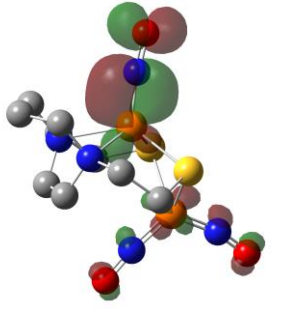
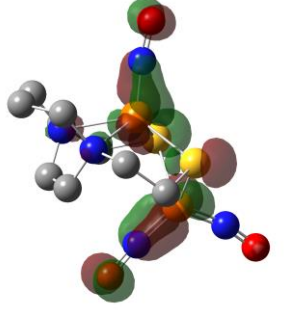
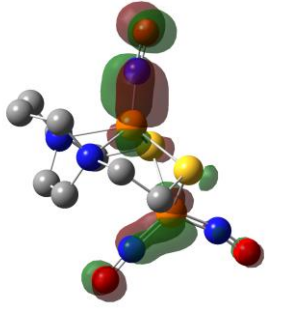
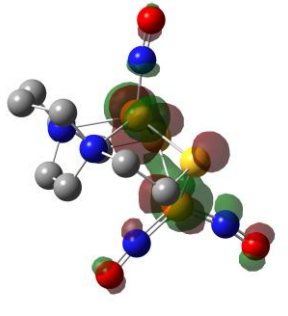
Supplementary Table 7. Reduction potentials as predicted by two basis sets.

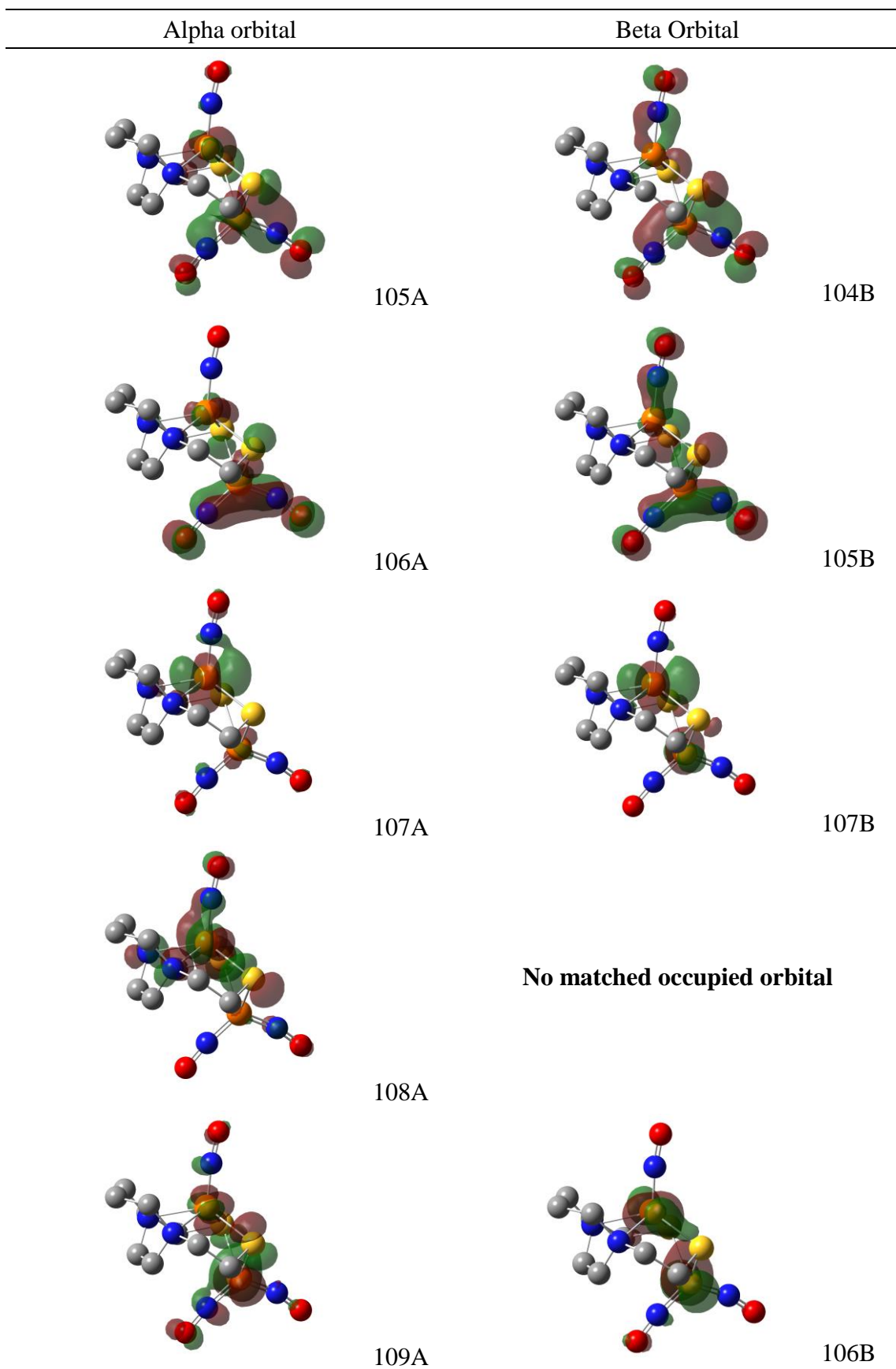
Basis Set	Reduction potential / V	
	1 st (1 ⁺ to 1 _{red})	2 nd (1 _{red} to 1 ⁻)
Exp.	-0.78	-1.41
All-e	-0.810	-2.08
ECP	-0.710	-1.66

Supplementary Table 8. Predicted spin densities of $\mathbf{1}^-$ by two basis sets.

Basis Set	Multiplicity	<i>S</i> value	Spin density			
			Fe ₄	NO	Fe ₄ (NO)	Fe(NO) ₂
All-e	Triplet	1.078	2.142	-0.523	1.619	0.088
ECP	Triplet	1.160	2.729	-0.883	1.846	0.042

Supplementary Table 9 . The alpha and beta occupied orbital matching for triplet 1^- .

Alpha orbital	Beta Orbital
 100A	 100B
 101A	 101B
 102A	 103B
 103A	 102B
 104A	No matched occupied orbital



Supplementary Note 1

The dependence of group state determination on basis sets. The results reported in the text were calculated by all-electron triple- ζ basis set 6-311++G(d,p).⁴ (The set is given an abbreviation All-e.) The method recently reported⁵ applies a mixed basis set: Stuttgart-Dresden double- ζ , effective core potential (SDD-ECP)⁶ on the irons, Los Alamos National Lab double- ζ , small-core ECP (LANL2DZ)⁷ on the sulfurs and 6-311++G(d,p) on the lighter atoms. (The set is given an abbreviation ECP.) Both data sets give very similar optimized geometric structures and IR frequencies. The major difference between them is the preference of multiplicity. ECP basis sets generally favor high-spin states, while all-electron, in contrast, prefers low-spin states.

The problem of ECP basis set is that, it introduces an unlikely quartet $\mathbf{1}_{\text{red}}$ as the ground state, which has an optimized geometry deviating from the crystal structure. The ECP basis set's tendency to favor high-spin, compared to the all-e basis set, is clearly shown on Supplementary Table 5. Selected metric parameters predicted by ECP are presented in Supplementary Table 6.

The dependence of calculated reduction potentials on basis sets. As mentioned in the text, the calculated redox event potential by all-e for the 2nd electron take-in has a deviation of 0.67V from the experimental value. Surprisingly, the ECP gives a rather good prediction of that potential. (Supplementary Table 7) The large deviation again is attributed to the multiplicity preference. The stability of triplet $\mathbf{1}^-$ is probably underestimated, resulting in a more negative reduction potential, requiring more energy to reduce $\mathbf{1}_{\text{red}}$.

The dependence of local spin densities on basis sets. In the preceding section, the Fe_1 in $\mathbf{1}^-$ is assigned as a nominally $S = 2$ high spin d^6 Fe(II), which should have an unsigned formal spin density of 4, while its bound NO is assigned a nominally $S = 1$ triplet NO^- along with an unsigned formal spin density of 2. Albeit, partial spin densities given by computations, as its analogous partial charges, follow this “formal assignment” pattern to a very limited extent. (Supplementary Table 8)

Interestingly enough, ECP's preference for high spin is not limited to the overall molecular spins, it even extends to the local spins or spin densities of molecular moieties: ECP tends to isolate alpha spin on one moiety of the molecule and beta on another to couple remotely rather to distribute electrons of opposite spins on the same MOs. As a consequence, the ECP basis set maximizes the spin polarization as possible and favors BS singlets over CS singlets in $\mathbf{1}^+$ case.

Supplementary Note 2

Additional explanation concerning the calculation concerning $\mathbf{1}_{\text{red}}^-$. In the following analysis, the plane formed by N_2S_2 is assigned as xy plane, and the nitrogens and sulfurs are placed on the angular bisectors of x and y axes (Supplementary Figure 4). For $\mathbf{1}_{\text{red}}$, the d_{xy} orbital on Fe_4 is vacant, as it is highly destabilized by donation from the N_2S_2 donors. With reduction of $\mathbf{1}_{\text{red}}$, the d_{xy} orbital accepts the added electron (assigned alpha spin for this discussion) and forms a triplet. To stabilize this orbital, Fe_4 rises out of the N_2S_2 plane to lower the overlap between the d_{xy} orbital of Fe_4 and the σ donor orbitals from N_2S_2 . However, this move also causes an increase in the overlap between doubly-occupied d_{xz} and d_{yz} orbitals and the σ donor orbitals from N_2S_2 , destabilizing these filled d orbitals. In $\mathbf{1}_{\text{red}}$, these d_{xz} and d_{yz} orbitals are nearly orthogonal to the σ donor orbitals from N_2S_2 and are strongly stabilized by, and delocalized into, the two π^* orbitals from NO. Once these xz and yz MOs are destabilized, they spin-polarize, leaving more alpha electron density on the d_{xz} and d_{yz} , and forcing beta electron density into the two NO π^* orbitals, resulting a nominally high-spin d^6 ($S = 2$) assignment on Fe_4 and a triplet-spin assignment on NO^- ($S = 1$), which now assumes a more linear structure.⁸ The nominally $S = 2$ $\text{Fe}_4(\text{II})$ and its bound $S = 1$ NO^- ligand are antiferromagnetically coupled to form an overall triplet as indicated by calculations. A sketch containing all the relevant geometric and electronic changes is presented in Supplementary Figure 4. In summary, the reduction from $\mathbf{1}_{\text{red}}$ to $\mathbf{1}^-$ adds one alpha electron on Fe_4 but also partially transfers two delocalized beta electrons from Fe_4 to the adjacent NO ligand, resulting in a theoretical net increase of spin density on Fe_4 greater than the one added electron. Here, the NO angle change in the second reduction event, from $\mathbf{1}_{\text{red}}$ to $\mathbf{1}^-$, is attributed to the conversion of ligand multiplicity, while that in the first reduction, from $\mathbf{1}^+$ to $\mathbf{1}_{\text{red}}$, is from the increased electron density alone. All in all, the geometry change of $\text{N}_2\text{S}_2\text{Fe}_4(\text{NO})$ is recognized as the interactive compromise between orbital energies and occupancy.

Contour plots of the spin orbitals and additional details of the calculations and other low-lying states can be found on Supplementary Table 9. There are two spin-polarized orbital pairs in $\mathbf{1}^-$: 102A / 103B and 103A / 102B. The major contributors to these two orbital pairs are d_{xz} , d_{yz} orbitals from Fe_4 and two π^* orbitals from the NO bound to Fe_4 . These orbitals are imperfectly matched because of the spin polarization which will be discussed in a separate section. The alpha electrons concentrate on d_{xz} and d_{yz} while beta electrons partially move more toward NO's two π^* orbitals. There are also two unmatched alpha orbitals, 104A and 108A, representing two singly filled d orbitals on Fe_4 .

Supplementary Methods

Reaction of $\mathbf{1_{red}}$ and $\mathbf{KC_8}$. Complex $\mathbf{1_{red}}$ (0.84 g, 0.20 mmol) and $\mathbf{KC_8}$ (0.03 g, 0.22 mmol) were loaded in a septum-sealed 50 mL Schlenk flask and 10 mL THF solvent was added to the reaction mixture at $-78\text{ }^\circ\text{C}$. The reaction mixture was stirred for 30 min; its IR spectrum (THF solution) found $\nu(\text{NO})$ bands at 1698 (s), 1654 (vs) cm^{-1} indicating the formation of reduced Roussin's Red Ester (rRRE) of presumed formulation $[\text{K}]_n[(\text{NO})_2\text{Fe}(\text{N}_2\text{S}_2)\text{Fe}(\text{NO})_2]_n$ ($n = 1$ or 2).⁹ Upon exposure to air, the rRRE was oxidized to $[(\text{NO})_2\text{Fe}(\text{N}_2\text{S}_2)\text{Fe}(\text{NO})_2]_n$ ($n = 1$ or 2) RRE (IR $\nu(\text{NO})$: 1810(w), 1775(vs), 1749(vs) cm^{-1}).¹⁰

The Detailed Calculation of Acid Dissociation Constant. For a Bronsted acid the $\text{p}K_a$ is calculated according to the following equations:

$$\begin{aligned} \text{HA} &= \text{A}^- + \text{H}^+ \\ \Delta_r G_m &= \Delta_r G_m^\theta + RT \ln \frac{[\text{A}^-][\text{H}^+]}{[\text{HA}]} \end{aligned} \quad (1)$$

When equilibrium is achieved,

$$\Delta_r G_m = 0 = \Delta_r G_m^\theta + RT \ln K_a \quad (2)$$

$$K_a = \exp\left(\frac{-\Delta_r G_m^\theta}{RT}\right) \quad (3)$$

$$\text{p}K_a = \lg e \frac{\Delta_r G_m^\theta}{RT} = 0.4343 \frac{\Delta_r G_m^\theta}{RT} \quad (4)$$

in which,

$$\Delta_r G_m^\theta = \Delta_f G_m^\theta(\text{H}^+) + \Delta_f G_m^\theta(\text{A}^-) - \Delta_f G_m^\theta(\text{HA}) \quad (5)$$

To the following reactions, exist

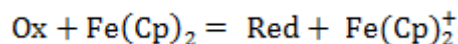
$$\begin{aligned} \mathbf{1H} &= \mathbf{1}^- + \text{H}^+ \\ \text{p}K_a(\mathbf{1H}) &= 0.4343 \frac{\Delta_f G_m^\theta(\text{H}^+) + \Delta_f G_m^\theta(\mathbf{1}^-) - \Delta_f G_m^\theta(\mathbf{1H})}{RT} \end{aligned} \quad (6)$$

$$\begin{aligned} \mathbf{1H}^+ &= \mathbf{1_{red}} + \text{H}^+ \\ \text{p}K_a(\mathbf{1H}^+) &= 0.4343 \frac{\Delta_f G_m^\theta(\text{H}^+) + \Delta_f G_m^\theta(\mathbf{1_{red}}) - \Delta_f G_m^\theta(\mathbf{1H}^+)}{RT} \end{aligned} \quad (7)$$

$$\begin{aligned} &\text{p}K_a(\mathbf{1H}) - \text{p}K_a(\mathbf{1H}^+) \\ &= 0.4343 \frac{\Delta_f G_m^\theta(\mathbf{1}^-) + \Delta_f G_m^\theta(\mathbf{1H}^+) - \Delta_f G_m^\theta(\mathbf{1H}) - \Delta_f G_m^\theta(\mathbf{1_{red}})}{RT} \end{aligned} \quad (8)$$

in which, $\Delta_f G_m^\theta$ is calculated by correcting electronic energy of target compound's optimal geometry, zero point and thermal motions in gas phase with PCM solvation model in CH_2Cl_2 . In this manner, the solvation problem of H^+ is avoided in the calculation.

Calculation of the Standard Electrode Potential. The standard electrode potential calculation was carried out using the corrected Gibbs free energy of formation mentioned above. When the following reaction



achieves equilibrium, there exists,

$$\Delta_r G_m = 0 = \Delta_r G_m^\theta + nFE^\theta \quad (9)$$

in which, E^θ is the electromotive force of the above chemical equation, F is Faraday constant and n is the number of electrons transferred (1 in our case). For the standard Gibbs free energy of reaction,

$$\Delta_r G_m^\theta = \Delta_f G_m^\theta (\text{Fe}(\text{Cp})_2^{\dagger}) + \Delta_f G_m^\theta (\text{Red}) - \Delta_f G_m^\theta (\text{Fe}(\text{Cp})_2) - \Delta_f G_m^\theta (\text{Ox}) \quad (10)$$

in which $\Delta_f G_m^\theta$ represents the standard Gibbs free energy of formation, which includes solvation correction. So that, E^θ can be presented as

$$\begin{aligned} E^\theta &= -\frac{\Delta_r G_m^\theta}{nF} \\ &= -\frac{\Delta_f G_m^\theta (\text{Fe}(\text{Cp})_2^{\dagger}) + \Delta_f G_m^\theta (\text{Red}) - \Delta_f G_m^\theta (\text{Fe}(\text{Cp})_2) - \Delta_f G_m^\theta (\text{Ox})}{nF} \end{aligned} \quad (11)$$

and as a primary battery, the electromotive force can be presented in another way as the combination of the electromotive forces of two half-reactions:

$$E^\theta = E^\theta(\text{Ox} / \text{Red}) - E^\theta(\text{Fe}(\text{Cp})_2^{\dagger} / \text{Fe}(\text{Cp})_2) \quad (12)$$

Since ferrocenium / ferrocene couple acts as the reference electrode, $E^\theta(\text{Fe}(\text{Cp})_2^{\dagger} / \text{Fe}(\text{Cp})_2)$ is set to 0 V. So that the standard electrode potential of the redox couple under investigation can be written as

$$\begin{aligned} E^\theta(\text{Ox} / \text{Red}) &= E^\theta \\ &= -\frac{\Delta_f G_m^\theta (\text{Fe}(\text{Cp})_2^{\dagger}) + \Delta_f G_m^\theta (\text{Red}) - \Delta_f G_m^\theta (\text{Fe}(\text{Cp})_2) - \Delta_f G_m^\theta (\text{Ox})}{nF} \end{aligned} \quad (13)$$

Supplementary References

1. Hsieh, C.-H., Darensbourg, M. Y. A $\{\text{Fe}(\text{NO})_3\}^{10}$ Trinitrosyliron Complex Stabilized by an N-Heterocyclic Carbene and the Cationic and Neutral $\{\text{Fe}(\text{NO})_2\}^{9/10}$ Products of Its NO Release. *J. Am. Chem. Soc.* **132**, 14118-14125 (2010).
2. Hess, J. L., Hsieh, C.-H., Reibenspies, J. H., Darensbourg, M. Y. N-Heterocyclic Carbene Ligands as Mimics of Imidazoles/Histidine for the Stabilization of Di- and Trinitrosyl Iron Complexes. *Inorg. Chem.* **50**, 8541-8552 (2011).
3. Hess, J. L., Conder, H. L., Green, K. N., Darensbourg, M. Y. Electronic Effects of $(\text{N}_2\text{S}_2)\text{M}(\text{NO})$ Complexes (M = Fe, Co) as Metallodithiolate Ligands. *Inorg. Chem.* **47**, 2056-2063 (2008).
4. Krishnan, R., Binkley, J. S., Seeger, R., Pople, J. A. Self-consistent molecular orbital methods. XX. A basis set for correlated wave functions. *J. Chem. Phys.* **72**, 650-654 (1980).
5. Brothers, S. M., Darensbourg, M. Y., Hall, M. B. Modeling Structures and Vibrational Frequencies for Dinitrosyl Iron Complexes (DNICs) with Density Functional Theory. *Inorg. Chem.* **50**, 8532-8540 (2011).
6. Chai, J.-D., Head-Gordon, M. Long-range corrected hybrid density functionals with damped atom-atom dispersion corrections. *Phys. Chem. Chem. Phys.* **10**, 6615-6620 (2008).
7. Kaupp, M., Schleyer, P. v. R., Stoll, H., Preuss, H. Pseudopotential approaches to Ca, Sr, and Ba hydrides. Why are some alkaline earth MX_2 compounds bent? *J. Chem. Phys.* **94**, 1360 (1991).
8. Ye, S., Neese, F. The Unusual Electronic Structure of Dinitrosyl Iron Complexes. *J. Am. Chem. Soc.* **132**, 3646-3647 (2010).
9. Lu, T.-T., Tsou, C.-C., Huang H.-W., Hsu I.-J., Chen, J.-M., Kuo, T.-S., Wang Y., Liaw W.-F., *Inorg. Chem.* **47**, 6040-6050 (2008).
10. Chiang, C.-Y., Miller, M. L., Reibenspies, J. H., Darensbourg, M. Y., *J. Am. Chem. Soc.*, **126**, 10867-10874 (2004).